Mesoscale Structure in the Megalopolitan Snowstorm, 11–12 February 1983. Part II: Doppler Radar Study of the New England Snowband

FREDERICK SANDERS

Center for Meteorology and Physical Oceanography, Massachusetts Institute of Technology, Cambridge, MA 02139

LANCE F. BOSART

Department of Atmospheric Science, State University of New York at Albany, Albany, NY 12222

(Manuscript received 2 January 1985, in final form 18 March 1985)

ABSTRACT

A major snowstorm in eastern Massachusetts, 11–12 February 1983, was associated with a persistent mesoscale band of high reflectivity observed at MIT. The band was strengthened, then weakened, by the propagation of a high-amplitude gravity wave through it, without permanent disruption of either entity. Transformation of a single band to a group of three accompanied rotation from zonal to northeast–southwest, as the storm passed eastward out of radar range.

An RHI cross section normal to the band at the inception of breakup showed a shallow layer of strong transverse (warm-to-cold) velocity components, evidently due to large-scale frontogenetical forcing, separating ascending air with small hydrostatic and symmetric stability above from descending air with large stability below. Band breakup was associated with a prominent small-scale oscillation along the transverse jet.

Vertical motions calculated from a velocity azimuth display time series showed descent in the layer from 1.5 to 2.5 km throughout the storm, with strong ascent and condensation present only well aloft. The storm-total overhead condensation, nevertheless, agreed closely with the storm-total snowfall.

Prominent fluctuation in the ascent reflected the passage of the gravity wave. Further unsteadiness of the ascent, and the breakup of the band, may have been attributable to symmetric instability.

1. Introduction

In the megalopolitan storm of 11–12 February 1983 (Sanders and Bosart, 1985; hereinafter referred to as SB) the heavy snow in the Boston area occurred as a synoptic-scale cyclone moved northeastward south of the New England coast. The snow was directly associated with a prominent mesoscale band observed on radar, oriented approximately along the tropospheric thermal wind. This paper presents a study of observations from the MIT radar. We wish to examine with these data the hypothesis advanced in SB that the band itself was due to large-scale frontogenetical forcing, while unsteady behavior, particularly in the upper portions of the synoptic-scale cloud mass, was attributable to symmetric instability. We also wish to show the effect on the snow band of a large-amplitude singular gravity wave investigated by Bosart and Sanders (1985; hereinafter referred to as BS), and to disclose other small-scale aspects of the storm and its precipitation amenable to detection by Doppler radar.

2. Constant-altitude plan-position indicator (CAPPI) maps

From the MIT WR-66 10 cm radar observations, a series of CAPPI maps of reflectivity was prepared at 15 min intervals from about 2030 GMT 11 February until about 1730 GMT 12 February, for the layers 0.5–1 km (960 to 900 mb) and 2.5–4 km (750 to 610 mb). Smoothed versions of these maps for selected times in the higher layer appear in Fig. 1. Cloud top isotherms from the satellite infrared imagery have been added, as have the centers of surface pressure rise and subsequent fall associated with the large-amplitude gravity wave (BS) when they were in range, and the surface observations from Logan Airport, Boston, MA (BOS), 6 km east of MIT.

The snow band moved from the south to MIT between 2130 and 0330 GMT at an average speed of 30 km h^{-1} (8.3 m s^{-1}), comparable to the southerly wind component in the layer from 2.5–4 km, as determined by Doppler velocities. The simple structure of the line began to be undone at 0230 GMT (Fig. 1c), when the approach of the gravity wave crest was associated with separate echo development to the south, and with a maximum of the reflectivity in the main band itself. The wake depression which immediately followed produced a fragmentation of the portion of the line west of MIT at 0330 and 0430 GMT (Figs. 1d and e), evidently because of subsidence in the snow-filled air. Subsequently, the crest propagated rapidly northeastward through the radar line, which had stopped at 0330 GMT. The line then

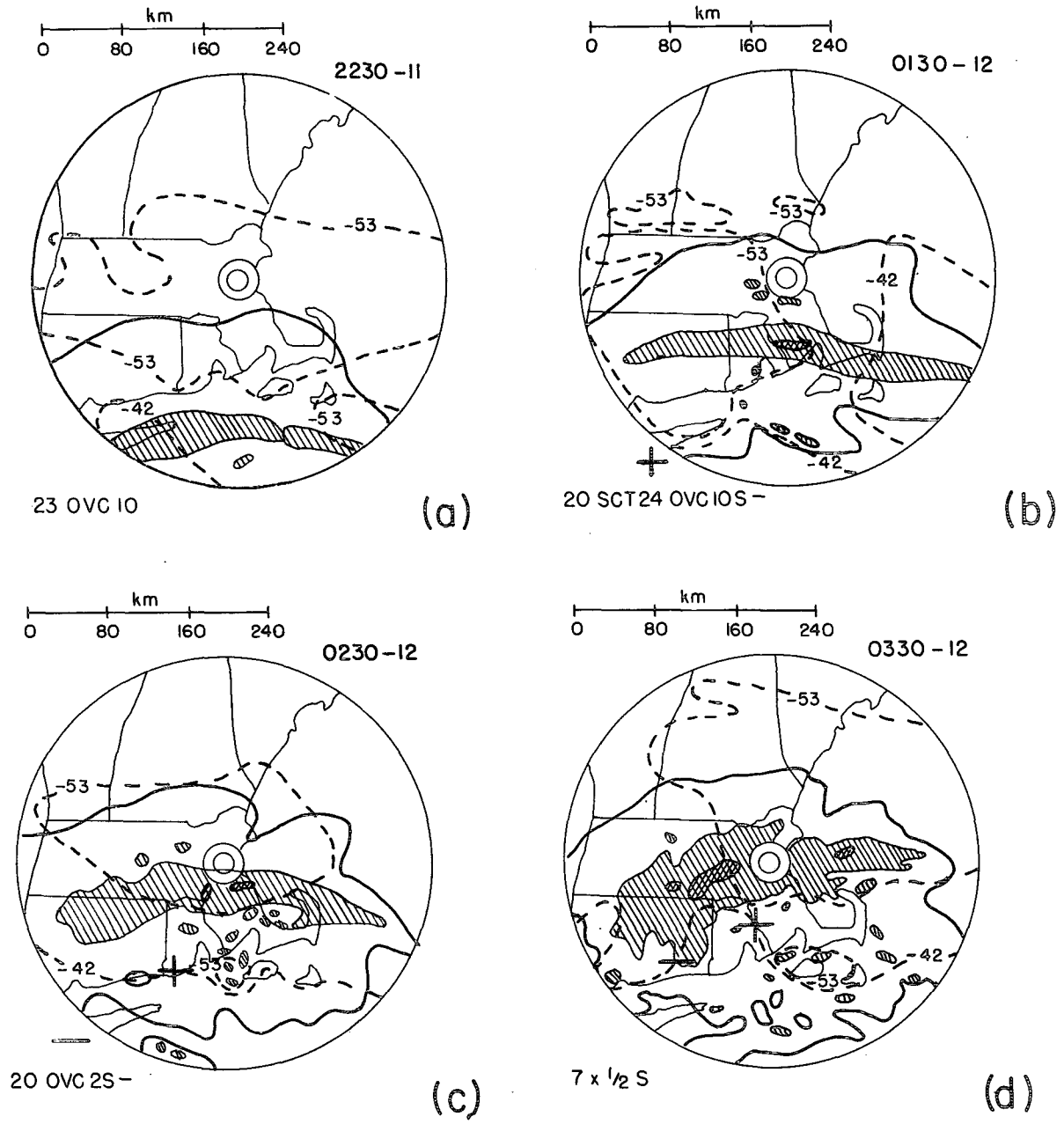

FIG. 1. Smoothed CAPPI maps for MIT radar at selected times (GMT) and dates (February) as indicated, for the layer from 2.5 to 4 km. Solid contours are for 15 dBZ, 25 dBZ (shaded), and 30 dBZ (cross-hatched). Dashed lines are cloud top isotherms, estimated from GOES infrared imagery, for 30 min after time of CAPPI map. Plus and minus signs show position of maximum rise and fall of surface pressure associated with the large-amplitude gravity wave. Heavy line on (h) (0730 GMT map) indicates position of RHI cross section shown in Fig. 2. Conventional surface observations at Boston, MA (BOS) 30 min after times of CAPPIs are added. Numerals I, II, and III in (h) and (i) denote persistent multiple bands.

strengthened and became reconsolidated at 0530 GMT (Fig. 1f) as the mesoscale depression moved eastward and dissipated. The heaviest snow was reported at BOS during this passage of the gravity wave, as at many other stations to the southwest (BS). Further complications arose immediately as the line, together with the thermal wind, began to rotate counterclockwise in response to the passage of the synoptic-scale cyclone. This development was accompanied by bifurcation of the line, as though it contained two centers of rotation, one east and one west of MIT. The development was partly obscured by a radar shadow extending northeastward from the transmitter, but the two lines (I and II) were clearly separated by

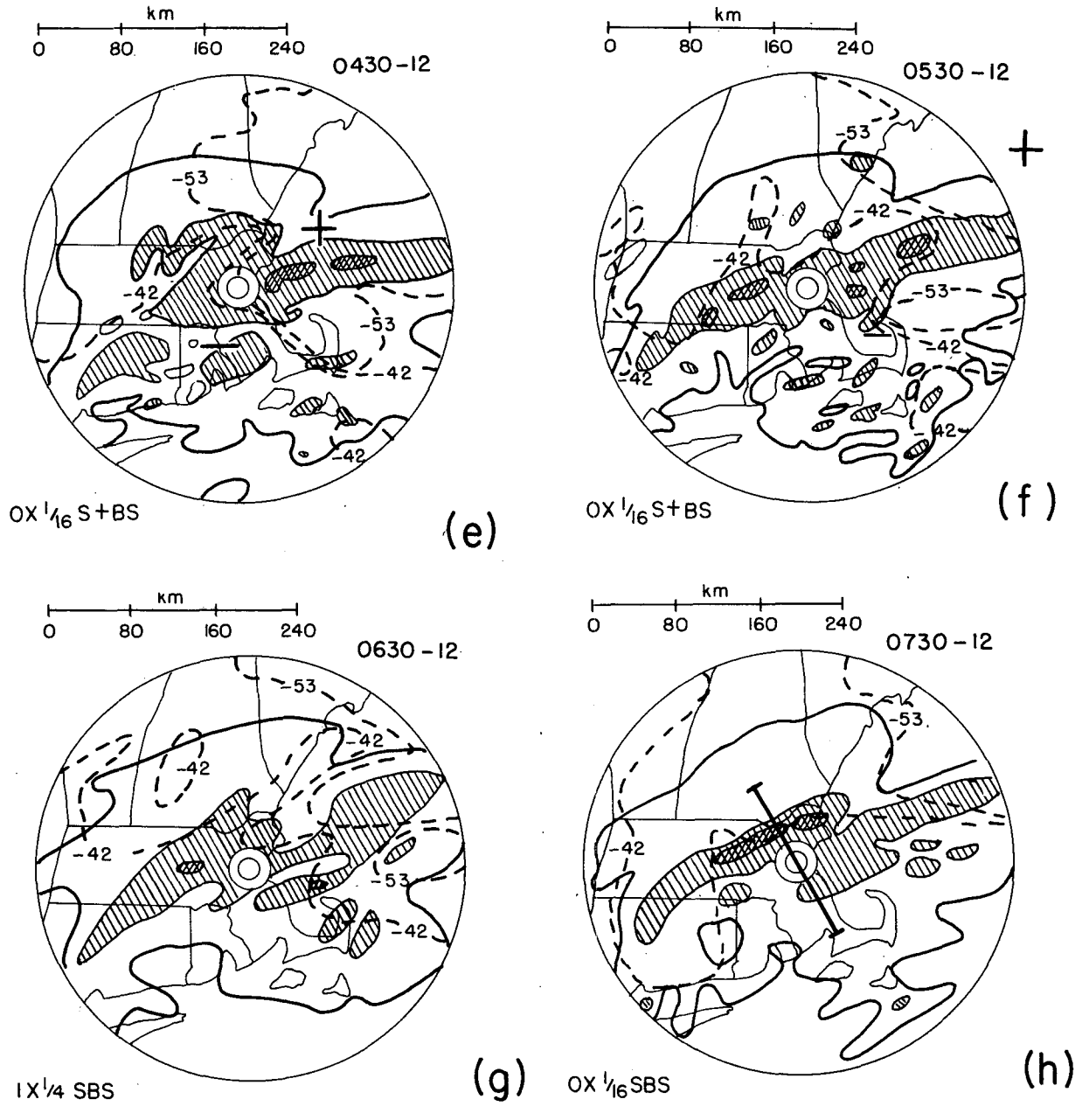

FIG. 1. (*Continued*)

1030 GMT, by which time a third (III) had developed as a northeastward-building segment. Finally, by 1330 GMT (Fig. 1j) as the snow virtually ceased (granted the difficulty in distinguishing, then, between falling and blowing snow), line I had moved slowly eastward, II had dissipated altogether, and III had moved more rapidly southeastward at 25 km h^{-1}.

The reasons for the behavior of the line are not clear. Why did the band stop when it reached the Boston area, despite a continuing southerly wind component above the surface boundary layer, as will be seen? The resulting extremely sharp northern edge of accumulated snowfall characterized the storm not only in eastern Massachusetts but, also well to the southwest (SB, Fig. 2b). Why did the atmosphere produce multiple bandedness after 0600 GMT?

The presence of the major band (or group of bands) within 150 km from MIT during the 15 h period illustrated in Fig. 1 implies a nearly continuous forcing, which the earlier analysis suggested was synoptic-scale frontogenesis. The earlier analysis, however, indicated that the upper-level response to the forcing was pulsed and discrete. Comparison in Fig. 1 of the satellite observed cloud top temperatures and the

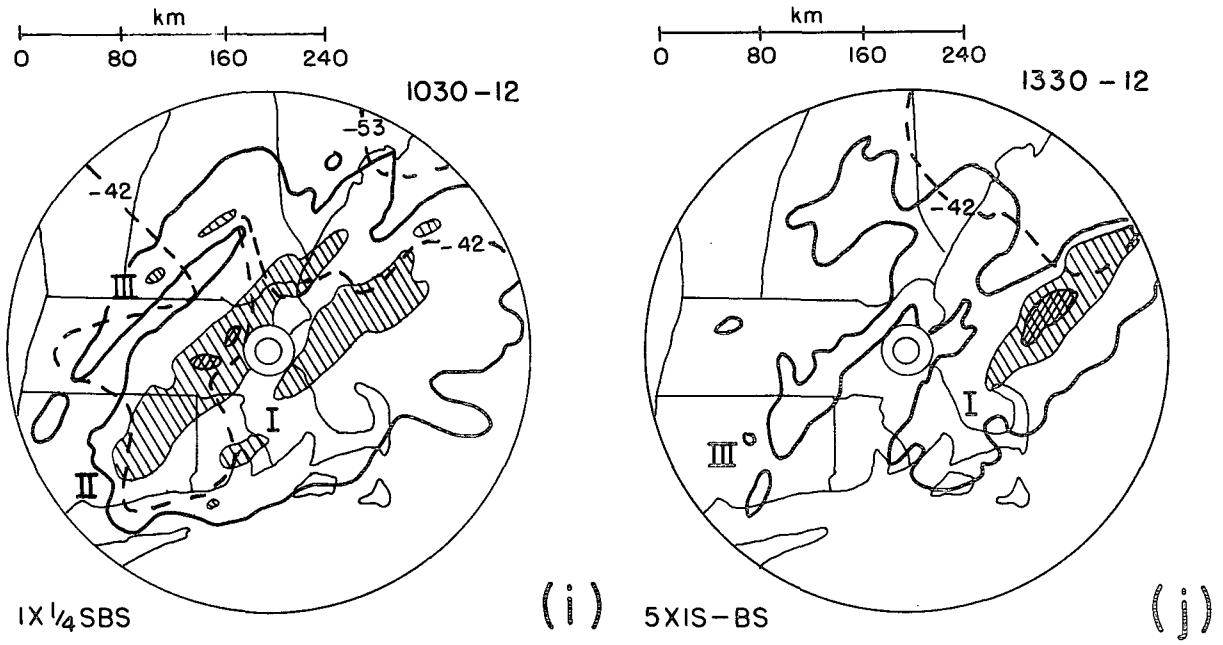

FIG. 1. (*Continued*)

radar reflectivity patterns shows that the two behaved mostly independently. Features of the former, particularly the cold patches, moved northeastward relative to the latter, evidently in response to the strong southwesterly winds in the upper troposphere, as discussed by SB. Note further in Fig. 1b the prominent appearance of a cold patch in the southwest, in advance of the approaching gravity wave crest. The effects of this wave were briefly detectable in both radar and cloud top patterns. The crest was clearly associated with a separate small cloud patch at 0230 GMT (Fig. 1c) as well as the convective-appearing echoes mentioned above. The depression was accompanied by a lowering of cloud tops to temperatures warmer than −42°C as well as by splintering of the reflectivity pattern. Elsewhere and otherwise, the details of the radar and cloud top patterns evolved independently. An attempt to infer surface precipitation from satellite imagery would face formidable difficulties.

These observations indicate a quasi-steady forcing and snowy response extending perhaps into the middle-tropospheric layer of small hydrostatic and symmetric stability, but an unsteady behavior of updraft and cloud mass in the upper troposphere where symmetric instability was likely (cf. SB).

3. A range–height indicator (RHI) view

At 0743 GMT an RHI sequence was begun, first toward the north-northwest and then toward the south-southeast, approximately normal to the evolving double band structure (Fig. 1h). This orientation is almost exactly normal to the tropospheric thermal wind interpolated between earlier and later rawinsonde analyses, hence along the x axis as SB defined it. A smoothed version of the reflectivity appears in Fig. 2 along with the Doppler radial components of velocity, the streamfunction defined as

$$\psi^x(p) = \int_p^{1000} u dp,$$

and the vertical motion ω^x. The u components for calculations of ψ^x were identified with the radial components and read from the RHI display as 50 mb layer averages at horizontal intervals of 10 km. The distinction between radial and u components becomes important at ranges less than 10 km, but had little impact on our calculations which did not use values at these short ranges. As a lower boundary condition, ψ^x was set equal to zero at the 1000 mb level.

A double-band structure can be seen in the reflectivity information in Fig. 2a, between $x = -60$ and -20 km and between $x = 0$ and 20 km, in reasonable accord with the CAPPI map obtained 15 min earlier (Fig. 1h). The Doppler radial speeds, viewed over the entire 160 km span in Fig. 2b, show a ribbon of strong negative u components (from warmer to colder air) embedded between the 3 km and 5 km levels. The strength was comparable to that observed from the sounding balloon near 4.5 km an hour earlier about 15 km to the west-northwest of MIT (cf. Fig. 9 in SB). The ribbon was most intense (near 28 m s^{-1}) between $x = 20$ and 60 km and weakest (about

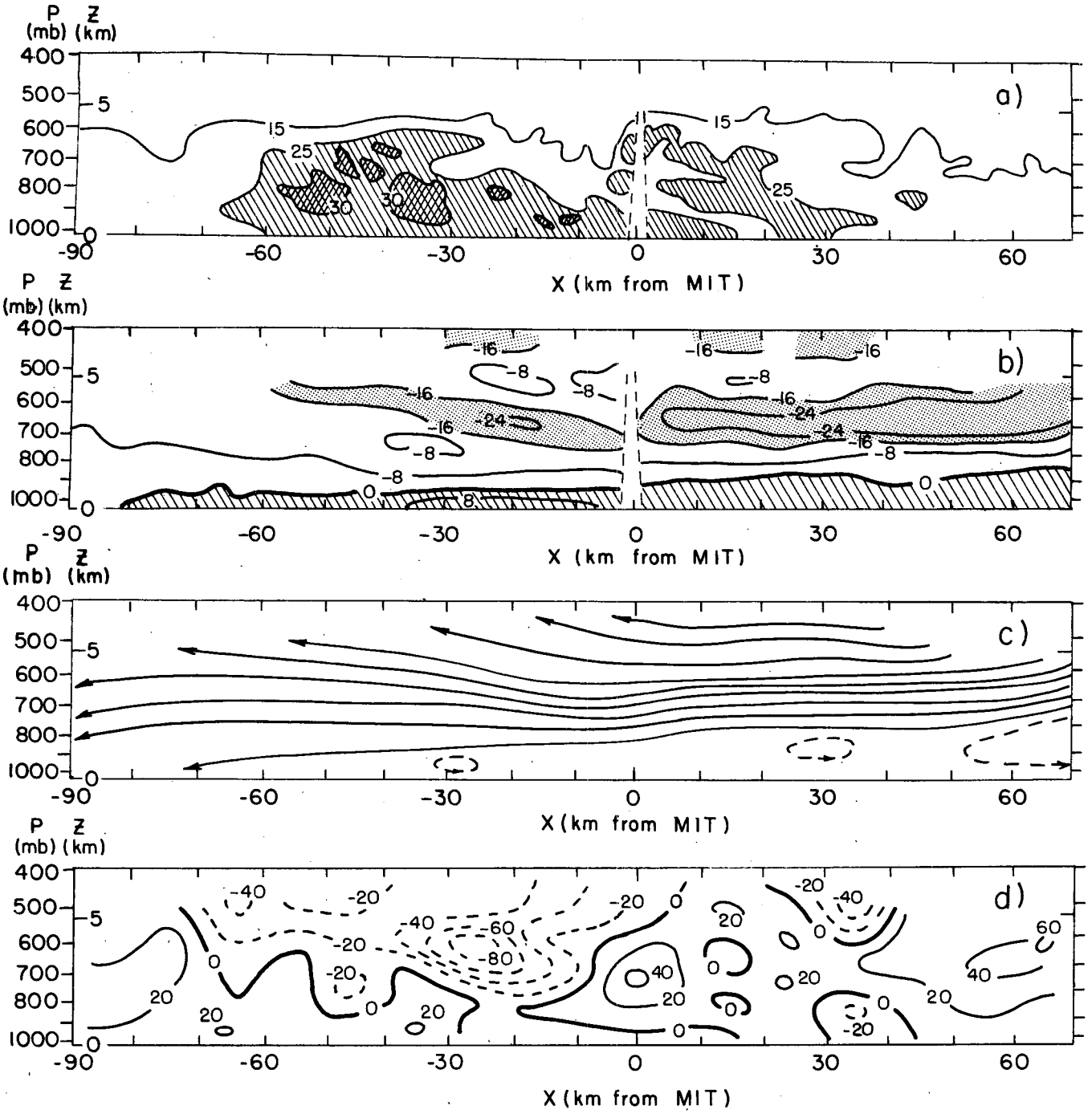

FIG. 2. RHI cross sections at 0743–0745 GMT 12 February: (a) radar reflectivity (dBZ); (b) radial component of wind, with isotachs at intervals of 8 m s^{-1}; (c) ψ^x (at intervals of 8×10^2 mb m s^{-1}); (d) ω^x (at intervals of 20×10^{-3} mb s^{-1}).

16 m s^{-1}) at its limit of detectability (near $x = -60$ km). It clearly resembles the ageostrophic wind-signature response to synoptic-scale frontogenetical forcing, seen in SB. The center of the ribbon approximately separated descending streamlines below from ascending ones above (as seen in Fig. 2c). The horizontally averaged vertical motions were modest, ranging from 13×10^{-3} mb s^{-1} at 750 mb ($w = -13$ cm s^{-1}) to -14×10^{-3} mb s^{-1} at 450 mb ($w = 24$ cm s^{-1}).

Prominent oscillations with wavelengths of the order of 30–60 km can be seen along the high speed ribbon in Fig. 2c. The vertical motions obtained by differencing ψ^x over 10 km distances (Fig. 2d) make

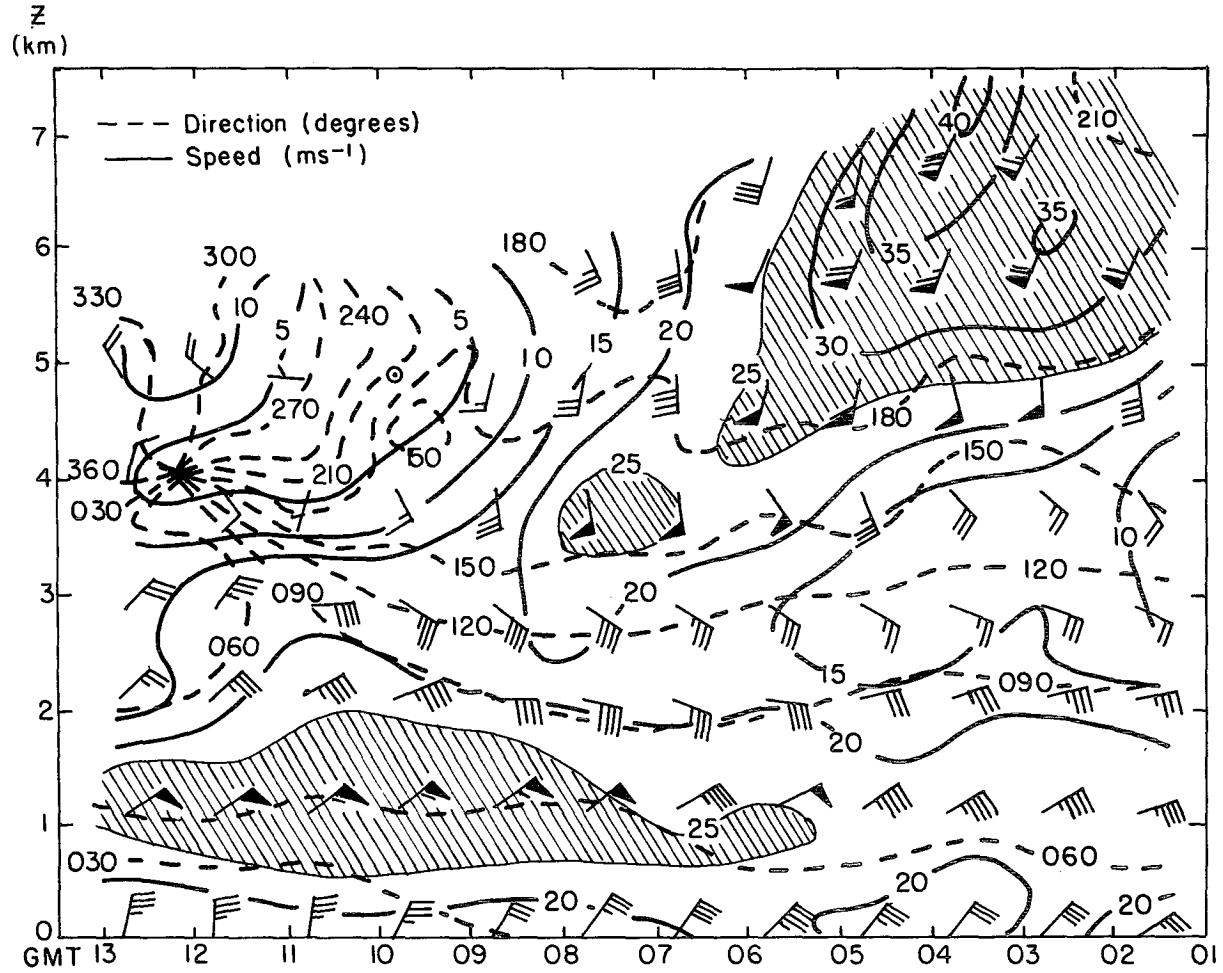

FIG. 3. VAD time-height sections from MIT radar 12 February: (a) direction (dashed isogons at intervals of 30 degrees) and speed (solid isotachs at intervals of 5 m s^{-1}); (b) vertical motion ω at intervals of 10×10^{-3} mb s^{-1}. Heavy dashed lines are levels of nondivergence. Column of numbers at right are standard deviation of divergence, in units of 10^{-5} s^{-1}; (c) condensation rate, in units of 10^{-6} g cm^{-2} s^{-1} for 50 mb layers. Column totals (in mm of liquid water h^{-1}) are shown along abscissa, denoted by Σ and accompanied by intensity of snow observed at Boston, MA (BOS).

these oscillations clearer. The u "jet" was descending from $x = 65$ to 25 km where reflectivity was relatively feeble. Weak ascent is seen at $x = 15$ just upwind from the weakening and southeast of MIT. Sharp descent of 40×10^{-3} mb s^{-1} ($w = -55$ cm s^{-1}) occurred more or less over MIT culminating in a zone of minimum reflectivity at $x = -10$ km, where band separation was occurring. Then, strong ascent with peak $\omega = -90 \times 10^{-3}$ mb s^{-1} ($w = 110$ cm s^{-1}) was seen at $x = -25$ km, upstream from the largest reflectivities in the section, in the vigorous band between $x = -30$ and -55 km. (The general descent beyond $x = -65$ km may have been overstated, since it is mainly the result of strong apparent divergence at the lowest levels. This is probably a spurious consequence of beam broadening and loss of shallow positive u components below the radar horizon at this range. Surface observations in and beyond this region showed northerly wind components.) Finally, maxima of ascent at the top of the Doppler data near $x = 35$ km and $x = -15$ km appear to be separate perturbations on another barely detectable streak of maximum negative u components at and above the 450 mb level. The prominent minima of radial component magnitude near 500 mb, and near 750 mb between $x = -25$ km and -40 km are further evidence of vertical layering.

Both this layering and the longitudinal oscillations in the cross-front circulation (associated with the band breakup in Fig. 1) indicate structure not explainable in terms of a single zone of frontogenetical forcing. Hoskins *et al.* (1984) have demonstrated the theoretical possibility of multiple frontal structure if large-scale frontogenesis operates on an initially irregular temperature field, but the multiple character is apparently shallow, contrary to our observations. Seltzer *et al.* (1985) have recently shown evidence for symmetric instability, in this case in the layer 2.5–

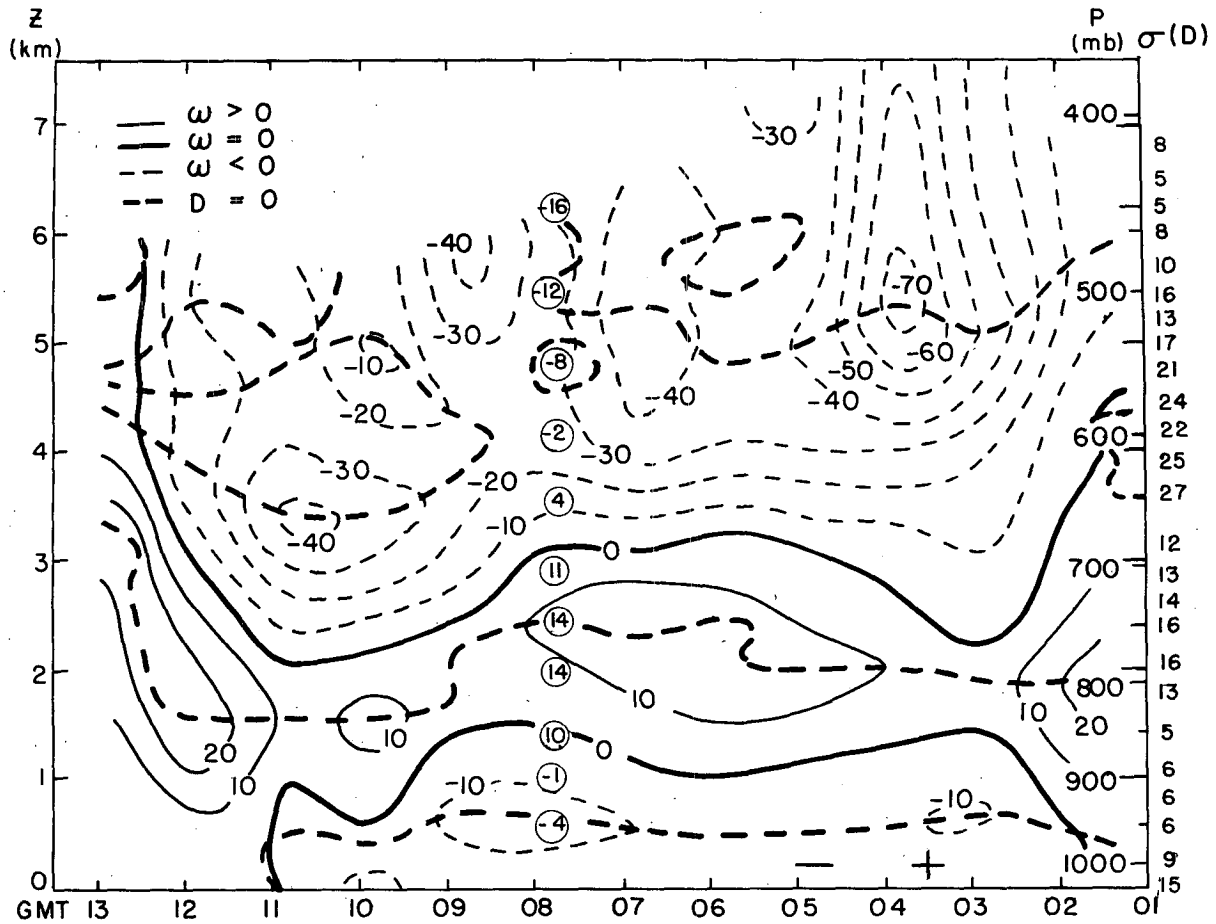

FIG. 3. (*Continued*)

5.25 km, but on the basis of the shear of the observed wind. Sanders and Bosart showed that this shear was highly ageostrophic, but that instability was present in about the same layer on a geostrophic basis. Seltzer *et al.* (1985) examined this case at a time when only a single precipitation band was visible on radar, but found in other cases an expected spacing between bands ranging from about 50 km to about 150 km. The observed layering implies a horizontal spacing near or above the upper limit of this range, while the oscillations and the multiple bandedness show spacing near the short end of the range and extend near or below the lower extremity of the unstable layer. Thus, while symmetric instability provides a plausible explanation of these irregularities, we cannot rule out other candidates.

4. Velocity azimuth displays (VADs)

The time history of the motion field and its implications for precipitation were obtained from a series of hourly VAD (Browning and Wexler, 1968) calculations through the duration of the storm, from 0145 to 1245 GMT. These refer to a vertical cylindrical volume with nominal radius 20 km centered at MIT, with data taken at vertical intervals of approximately 300 m. (To provide this vertical resolution up to 6.8 km with the limited available number of scanning elevation angles up to 15 degrees, it was necessary to use radii ranging from 14–26 km.) A vertical time section of area-averaged wind direction and speed is shown in Fig. 3a. Some subjective judgment was used at both the base and the top of the display. At the bottom, points in the northeast sector were found to represent return from high waves in Massachusetts Bay (visible because of the high altitude of the radar, not an alarming sea state) and were ignored. The upper limit was taken as the highest elevation at which data points were available in more than half of the 30° sectors comprising the circle. The assumed quasi-sinusoidal variation of radial wind component with azimuth was used as a guide in analysis of these marginal circles, where the uncertainty is relatively large. In Fig. 3a we see that northeasterly winds occurred throughout the storm at and below 1 km, becoming generally stronger with time. In all but the latest part, the wind veered with elevation, reaching south or south-southwest around 5 km. Maximum speed in this southerly current descended and weak-

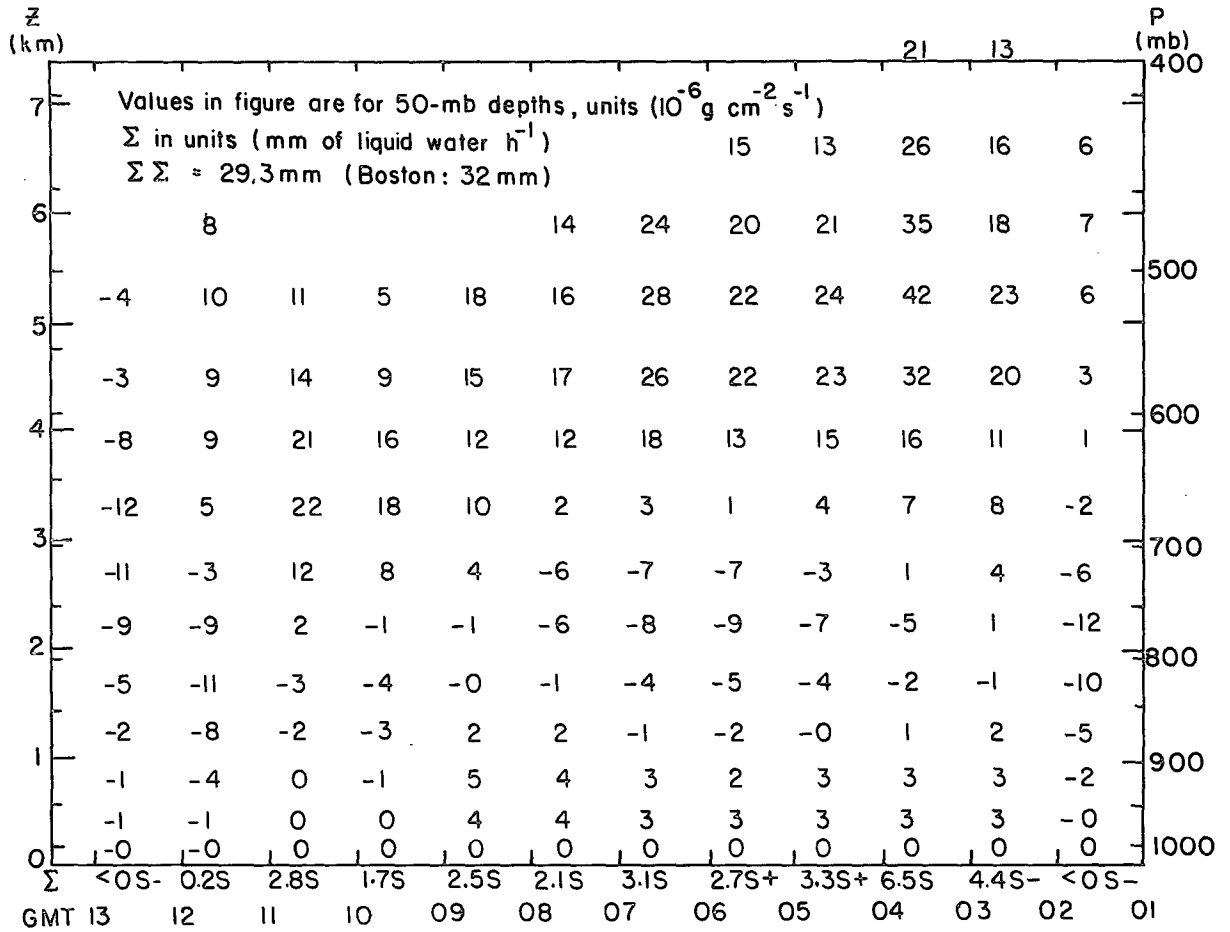

FIG. 3. (*Continued*)

ened with time, the jet-like character disappearing after 0800 GMT. This feature doubtless corresponds to the wind signature seen in the 0600 GMT sounding (SB, Fig. 9) from MIT (actually made between 0549 and 0651 GMT), and in the RHI depiction at 0744 GMT (Fig. 2b). The local maximum near 6 km at about 0300 GMT may be associated with the separate maximum observed in the 0000 GMT MIT sounding. Light winds prevailed above 3 km after 0900 GMT as the upper trough passed overhead.

Divergence was calculated for the same volume, and vertical motion ω was obtained by integrating it upward from the elevation of the transmitter, where ω was assumed to be zero. Results are seen in Fig. 3b. Between 0200 and 1100 GMT, weak ascent extended up to 1 km. Above this, weak descent persisted to elevations of 2 or 3 km, adjoining stronger descent before and after this period; then ascent extended up to the upper limit of Doppler information. There was much structure in this region of prominent ascent. The major maximum at about 5.5 km and 0400 GMT followed by a relative minimum 2 h later was matched by parallel behavior in the descent region below. This fluctuation appears to be attributable to the gravity wave crest and depression propagating northeastward near MIT (cf. Fig. 1). A number of less dramatic pulses of upward motion can be seen until the end of general ascent after 1200 GMT.

Comparison of the VAD result at 0746 LST with the RHI data taken immediately before shows similar variation with elevation, but a positive bias in the latter of about 10×10^{-3} mb s^{-1}. This was attributable mainly to the inability of the RHI display to detect the strong convergence near the ground. Its representation, as mentioned, required subjective interpretation.

To the eye, the vertical motion seems relatively steady in time up to 3.5 km, above which unsteadiness is the rule. This appearance is consistent with the idea advanced previously of a steady response to frontogenetical forcing in the lower region of large symmetric stability and an unsteady one in the upper region of small stability. Lest the effect be merely the result of randomly accumulating error in an upward integration of divergence, we calculated the standard

deviation of the divergence values in time at each level. The result, in Fig. 3b, supports the idea of a sudden onset of large variability at an elevation of 3.5 km (650 mb), just above the transition to low stability in the MIT sounding at 0600 GMT, seen in SB Fig. 9.

In view of the importance of accretion of preexisting condensate in the total precipitation recorded at the ground in CYCLES Project cases, as compared presumably to local condensation in the overhead air column (Herzegh and Hobbs, 1980; Hobbs *et al.*, 1980; Herzegh and Hobbs, 1981; Houze *et al.*, 1981), it is of interest to calculate the condensation implied by Fig. 3b. Saturation was assumed at all levels, while the necessary temperature profile was obtained from the 0000 GMT MIT sounding for the first two times and from the 0600 GMT sounding thereafter. In the regions of descent, sufficient evaporation was assumed to keep the air saturated.

Results are displayed in Fig. 3c, for 50 mb layers and for the column totals. The condensation rates, of course, follow the vertical motions closely, with some diminution at high elevations due to lessening of the rate of change of saturation mixing ratio along a moist adiabat. Still, substantial condensation was occurring at the upper limit of detectable reflectivity at and above the 400 mb level.

The column totals suffer from two opposing sources of bias. The rates for individual layers and times are slightly overstated because they were calculated on the basis of saturation vapor pressure for liquid water, whereas the storm, being composed entirely of snow, required more nearly the lower saturation pressure for ice. On the other hand, the calculations did not extend to the upper limit of condensation. As neither of these flaws appears to be egregiously larger than the other, the hourly column totals appear reasonably reliable. The calculated storm-total condensation (the sum of all the positive column totals) is 29.3 mm, which compares favorably with 32 mm reported at BOS and with other nearby values (cf. SB, Fig. 2). Therefore, so far as the storm-total precipitation over the 40 km diameter circle centered at MIT is concerned, convergence of transport of condensate appears to have been of little consequence. Moreover, in contrast to the Pacific Coast storms, massive condensation occurred above 5 km, with net evaporation below 3 km. Thus, the "seeder-feeder" mechanism so prominent in the CYCLES cases, if present here at all, must have operated on extremely small space and time scales, and had little overall importance. This mechanism requires major precipitation growth in the lower troposphere. This can occur by scavenging cloud that is either generated *in situ* or is transported from the environment. In the former case, one would have ascent in the lower levels; in the latter a deficit of condensation relative to precipitation. We see neither. On the whole, the descent in the layer from 1–3 km robbed snow enthusiasts of some 4 or 5 cm that might otherwise have reached ground.

Comparison of the hourly condensation totals with the surface observations at BOS, however, provides us with assurance that cloud physics had an effect. Light snow was reported at 0200 GMT, with visibility 17 km when the calculated total was negative, slight condensation in the cloud above 650 mb being overbalanced by evaporation below. Two possibilities may explain the discrepancy. The evaporation may be overestimated; or snow transported horizontally, either in the upper cloud deck or in the lower boundary layer cloud (cf. SB, Fig. 8a), may have been falling out. Largest condensation totals were calculated at 0300 and 0400 GMT, while heaviest snow was reported the following two hours. Much of the condensation was occurring in a powerful updraft (0.5–1 m s^{-1}) at and above 5 km. Since snow crystals fall at speeds near 1 m s^{-1}, it seems likely that most of the 2 h delay represented the time necessary for this heavy concentration of condensate to reach the ground. (Since the snow crystals would have migrated horizontally some tens of km during this time, it is necessary to assume that the calculated condensation represented, reasonably well, conditions beyond the 20 km circle of the VAD measurements.) The reported rate of accumulation of snow at BOS was more or less uniformly great (2.5–5.0 cm h^{-1}) through 1200 GMT, but growth of depth probably depended as much on drifting and blowing as on falling snow, and was notoriously difficult to measure in any case, during this period of high wind. It would not, therefore, be highly correlated with condensation. Finally, light snow continued to be reported for two hours after the column-total condensation rate returned to negative. This discrepancy was probably attributable to existing condensate falling out from above and blowing in from the northeast.

5. Concluding discussion

We have studied this major snowstorm through analysis of reflectivity and Doppler velocity information from radar. The heavy snow at Boston was associated with a pronounced mesoscale band of high reflectivity which remained nearly stationary for many hours, being first locally intensified and then temporarily disrupted by the passage of a high-amplitude gravity wave. The single band was gradually transformed into a group of three parallel bands, spaced about 70 km apart, accompanied by reorientation from approximately zonal to northeast-southwest. Finally, the group moved off toward the east as did the accompanying synoptic-scale cyclone. The radar band was not well correlated with the coldest (thus highest) tops in the synoptic-scale cloud system, as seen in satellite infrared imagery. These high tops

overlay the band during the onset of heavy snow at the ground, but had advanced far to the northeast as much of the snow fell.

An RHI cross section approximately normal to the thermal wind showed a prominent ribbon of maximum transverse velocity components, from warmer toward colder air, with a vertical half-width of about 1 km and a suggestion of a second, weaker maximum near the top of radar detectability. The concentrated transverse velocity components appear to be a response to large-scale frontogenetical forcing accompanied by small symmetric stability in the warmer air. The radar band was evidently produced by this intense sloping updraft. At the time of the RHI, the breakup of the single radar band was beginning and appeared to be accompanied by prominent oscillations of vertical motion along the transverse ribbon. The most intense ascent lay just upstream from the highest reflectivities in the strongest radar band. The vertical structure and the transverse oscillations may have been manifestations of symmetric instability.

The time series of Doppler VAD wind profiles for a circle with nominal radius 20 km, centered at MIT, showed that the ribbon of strong warm-to-cold flow weakened and descended from elevations near 7 km at the outset of the storm, to about 3 km, becoming indistinct near the end of the heavier snow.

Kinematic vertical motions derived from the VAD divergences showed that a layer of modest descent (about 10 cm s^{-1}), centered between 1.5 and 2.5 km, was present throughout the storm, representing presumably the descending cold-to-warm branch of the frontal circulation. Strong ascent (at least 30 cm s^{-1}) began at elevations ranging from 4 km at the beginning of the storm to 2.5 km near the end.

A study of condensation rates based on soundings and Doppler data at MIT showed that storm-total condensation compared favorably to observed precipitation. The beginning and ending of snow, however, and the timing of the heaviest fall, could not be understood without taking account of the modest fall velocity of snow crystals. It would be interesting to know whether these characteristics are typical of East Coast storms, since if so they could differ systematically from West Coast storms, in which the "seeder-feeder" scavenging mechanism evidently plays an important role.

Acknowledgments. We are grateful to Kerry Emanuel for provocative comments and fruitful discussion, and to Isabelle Kole for the drafting of illustrations. Special thanks are due to Rich Passarelli for many contributions to this work, ranging from initiating the addition of Doppler capability to the MIT radar, without which the investigation would not have been undertaken, to arguing cogently with us about interpretation of the results. This work was supported by the National Science Foundation under Grant numbers ATM-801930 (MIT), ATM-8209375 (MIT), and ATM-8026557 (SUNYA).

REFERENCES

Bosart, L. F., and F. Sanders, 1985: Mesoscale structure in the megalopolitan snowstorm of 11–12 February 1983. Part III: A large-amplitude gravity wave and coastal frontogenesis. Submitted to *J. Atmos. Sci.*

Browning, K. A., and R. Wexler, 1968: A determination of kinematic properties of a wind field using Doppler radar. *J. Appl. Meteor.*, **7**, 105–113.

Herzegh, P. H., and P. V. Hobbs, 1980: The mesoscale and microscale structure and organization of clouds and precipitation in midlatitude cyclones. II: Warm frontal clouds. *J. Atmos. Sci.*, **37**, 597–611.

——, and P. V. Hobbs, 1981: Mesoscale and microscale structure and organization of clouds and precipitation in midlatitude cyclones. IV: Vertical air motions and microphysical structures of prefrontal surge clouds and cold-frontal clouds. *J. Atmos. Sci.*, **38**, 1771–1784.

Hobbs, P. V., T. J. Matejka, P. H. Herzegh, J. D. Locatelli and R. A. Houze, Jr., 1980: The mesoscale and microscale structure and organization of clouds and precipitation in midlatitude cyclones. *J. Atmos. Sci.*, **37**, 568–596.

Hoskins, B. J., E. C. Neto and H.-R. Cho, 1984: The formation of multiple fronts. *Quart. J. Roy. Meteor. Soc.*, **110**, 881–896.

Houze, R. A., Jr., S. A. Rutledge, T. J. Matejka and P. V. Hobbs, 1981: The mesoscale and microscale structure and organization for clouds and precipitation in midlatitude cyclones. III: Air motions and precipitation growth in a warm-frontal rainband. *J. Atmos. Sci.*, **38**, 639–649.

Seltzer, M. A., and R. E. Passarelli, Jr. and K. E. Emanuel, 1985: The possible role of symmetric instability in the formation of precipitation bands. Submitted to *Mon. Wea. Rev.*

Sanders, F., and L. F. Bosart, 1985: Mesoscale structure in the megalopolitan snowstorm of 11–12 February 1983. Part I: Frontogenetical forcing and symmetric instability. **42**, 1050–1061.